Preliminary U-Pb geochronology of the Tugela terrane, Natal belt, eastern South Africa

Stephen T. Johnston[1], Richard Armstrong[2], Larry Heaman[3],
Steve McCourt[4], Andrew Mitchell[4], Avi Bisnath[4] and Makoto Arima[5]

[1]*School of Earth and Ocean Sciences, University of Victoria, PO Box 3055 STN CSC,
Victoria, British Columbia, V8W 3P6 Canada*
[2]*Research School of Earth Sciences, The Australian National University, Canberra,
ACT 0200, Australia*
[3]*Department of Earth and Atmospheric Sciences, University of Alberta,
Edmonton, Alberta, T6G 2E3 Canada*
[4]*School of Physical Sciences, University of Durban-Westville, Private Bag X54001,
Durban 4000, South Africa*
[5]*Geological Institute, Yokohama National University, Hodogaya-ku,
Yokohama 240-8501*

Abstract: We report on the preliminary results of a geochronological study of the Tugela terrane, the northernmost tectonic element of the Mesoproterozoic Natal belt of eastern South Africa. The Tugela terrane consists of a west-plunging structural stack, with the structurally highest, most allochthonous and presumably most oceanic tectonostratigraphic packages exposed to the west. Our study focused on the three highest tectonostratigraphic packages. These are, from west to east, the Tugela, Mandleni and Madidima, respectively. The Tugela tectonostratigraphic package consists of an oceanic arc sequence, including arc tholeiites and a tonalite intrusion (the Kotongweni tonalite gneiss). The Mandleni tectonostratigraphic package is characterized by a geochemically enriched bimodal magmatic succession (the Dondwana tectonite unit). Metasedimentary rocks comprise the Madidima tectonostratigraphic package, including the feldspathic Dulumbe paragneiss. All the thrust sheets are characterized by a penetrative schistosity/gneissosity, and by synkinematic upper amphibolite to granulite grade metamorphism. Voluminous mafic to ultramafic magmatism, including the emplacement of the Tugela Rand complex, the Mkondene diorite and the Mambula complex, which is characterized by massif anorthosite, occurred late during this tectonic event. Subsequent exhumation and lower amphibolite grade metamorphism was coeval with the development of north-verging folds and thrust faults, tectonic interleaving of the terrane with ophiolite, and voluminous granitic magmatism (the Wosi granitoid suite).

U-Pb zircon age determinations constrain the age of the metasedimentary Dulumbe paragneiss to being post-1276±10 Ma, the age of the oldest detrital component in the sequence. The lack of any older detrital zircons suggests that the Tugela terrane was far-removed from the Archaean Kaapvaal craton during deposition. Oceanic magmatic arc development was underway by 1209±5 Ma, the age of the protolith of the Kotongweni tonalite gneiss. Subsequent crustal thickening and tectonic burial of the terrane occurred prior to about 1180 Ma, the age of intrusion of the late to post-tectonic Mkondene diorite and the Mambula complex. Peak metamorphism occurred at 1175±9 Ma, the age of metamorphic zircon, and inherited zircons that had suffered syn-metamorphic Pb-loss in the Dulumbe paragneiss. Subsequent exhumation and

northward obduction of the terrane, occurred at around 1155±1 Ma, the age of syn-tectonic intrusions of the Wosi granitoid suite.

key words: South Africa, tectonics, magmaticarc, Kibaran-Grenvillian, Rodinia

1. Introduction

Mesoproterozoic orogenic belts are common to most continental fragments. This observation, in part, led to the suggestion that the orogenic belts provide a record of the construction of a latest Mesoproterozoic to Neoproterozoic supercontinent–Rodinia (Hoffman, 1991). Attempted reconstructions of Rodinia have relied upon the use of pinning points formed where the Mesoproterozoic orogenic belts are truncated against younger orogenic belts, and against the margins of present day continental blocks. The Mesoproterozoic Natal belt of eastern South Africa provides a particularly robust pinning point (Fig. 1). The belt is truncated to the east against the Indian Ocean margin of the African continent, and consists of, from south to north, the Margate, Mzumbe and Tugela terranes, respectively. The Margate and Mzumbe terranes are characterized by abundant granitoid gneisses and have been interpreted as magmatic arcs (Thomas, 1989). The heterogeneous Tugela terrane includes metabasite, ultramafic and silicic intrusions, and metasedimentary sequences. Although previously interpreted as oceanic crust that floored an ocean basin lying north of the Mzumbe and Margate magmatic arcs (Matthews, 1972), more recent mapping and geochemical studies (Arima *et al.*, 2001; Johnston *et al.*, 2001) are consistent with the presence of arc and rift assemblages within the terrane. The Tugela terrane lies in structural contact to the north with Archaean strata of the Kaapvaal
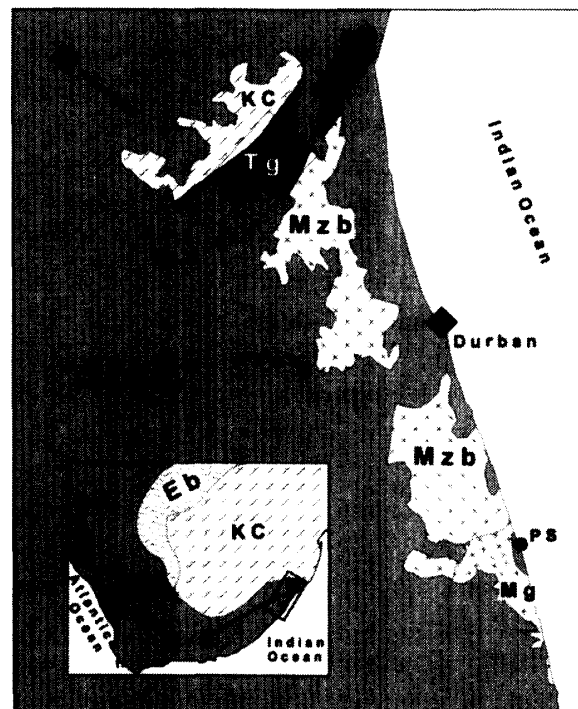
Fig. 1. Regional geology of the Natal belt. Figure location is indicated in the location map, inset at lower left. Geological provinces include: N-N–Namaqua–Natal belts, Eb–Eburnian (Kheis belt), KC–Kaapvaal craton, Mg–Margate terrane, Mzb–Mzumbe terrane, Tg–Tugela terrane. Cities include: Pmb–Pietermaritzburg; and PS — Port Shepstone

craton (Fig. 1).

Although a well-defined pinning point, no satisfactory match has yet been located upon for the Natal belt upon any other continental block. Part of the problem lies in the poorly defined tectonic and geological evolution of the Natal belt. In particular there is a dearth of high quality U-Pb geochronological age determinations. Studies in progress in the Mzumbe and Margate terranes (Johnston *et al.*, in preparation; Thomas *et al.*, 1999; B. Eglington *et al.*, unpublished data) are helping to clarify the evolution of the arc terranes. Recent mapping and geochemical studies of the Tugela terrane (Arima *et al.*, 2001; Johnston *et al.*, 2001) have helped define the tectonostratigraphic elements that constitute the terrane, and place constraints on their origin. Here we report the preliminary results of a geochronological study aimed at providing temporal constraints on the evolution of the Tugela terrane, and further elucidating the tectonic evolution of the Natal belt.

2. Stratigraphy

The Tugela terrane forms a west-plunging thrust stack (Matthews and Charlesworth, 1981) consisting of four tectonostratigraphic packages – the Nkomo, Madidima, Mandleni and Tugela, respectively from east to west (Fig. 2). Structurally deep levels in the east have been interpreted as parauthochthonous strata thought to be closely linked to the more northerly Kaapvaal craton; structurally shallow levels exposed to the west are thought to be highly allochthonous and are presumed to be the most oceanic elements of the terrane (Matthews, 1972). In this paper we focus on the uppermost tectonostratigraphic packages of the terrane, the Tugela, Mandleni and Madidima (Figs. 2, 3), and on the Wosi granitoid suite, a voluminous set of granitoid sills and dykes, that intrude all three tectonostratigraphic packages.

2.1. Tugela tectonostratigraphic package

The Tugela tectonostratigraphic package (TTP) is the highest structural element within the Tugela terrane. Much of the package is underlain by the Manyani amphibolite, a unit that includes amphibolite, amphibolitic gneiss and tremolite-chlorite schist. Lesser amounts of felsic gneiss, and rare layers of magnetite quartzite and dolomite are interfoliated with the metabasites. A homogeneous garnet hornblende tonalite gneiss is referred to as the Kontongweni tonalite (Harmer, 1979) (Fig. 2). Although strongly lineated and foliated, the intrusive contact of the orthogneiss with its amphibolitic wall rocks remains recognizable, as are wallrock xenoliths within the intrusion. Mapping and geochemical data have demonstrated that the Manyani amphibolites were derived from low-K tholeiitic basaltic rocks chemically similar to those being generated in modern oceanic arcs (for example, in the Izu-Bonin arc). The Kotongweni tonalite gneiss is an extremely depleted M-type granitoid, with very low abundances of K, Rb, rare earth and large ion lithophile elements. N-MORB normalised spidergrams exhibit features considered diagnostic of arc-related intrusions, and is similar to the Phanerozoic Tanzawa tonalite of the Izu-Bonin arc (Arima *et al.*, 2001; Johnston *et al.*, 1998). These findings are consistent with interpretation of the Manyani amphibolites and the Kotongweni tonalite gneiss as being the volcanic and plutonic elements of a
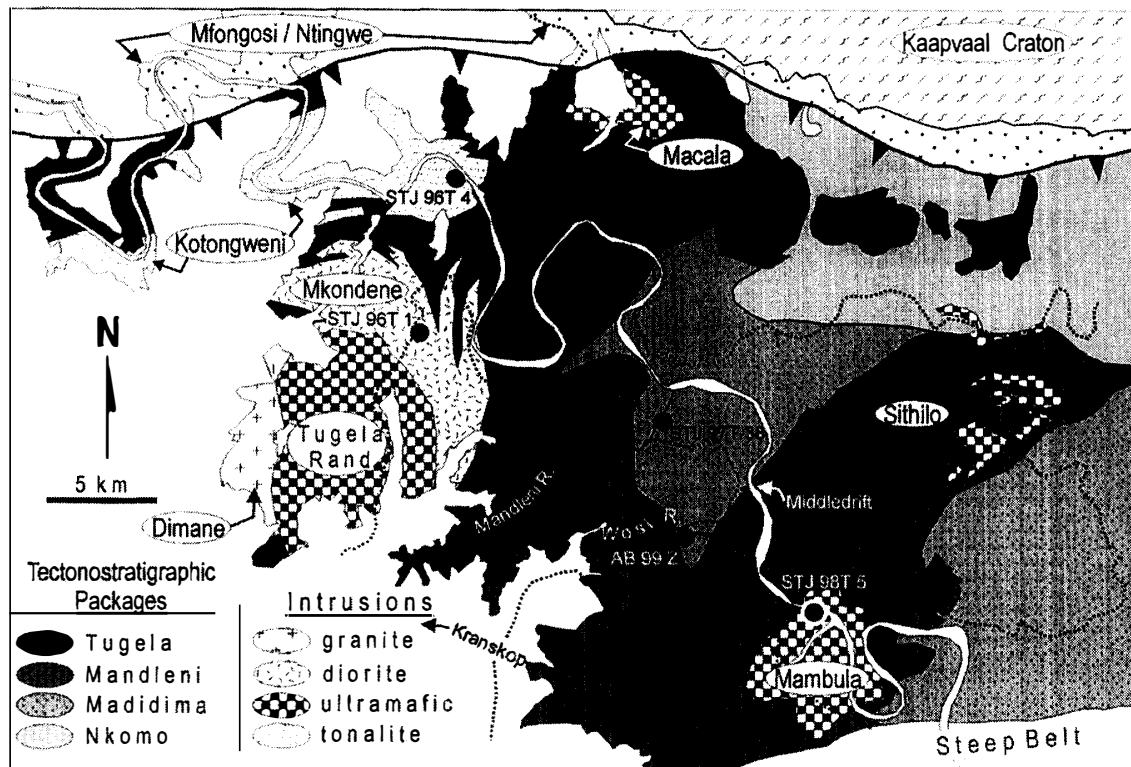
Fig. 2. Detailed geology of the Tugela terrane. Map location indicated in Fig. 1. Sample locations are indicated by filled dots. The Tugela tectonostratigraphic package includes the Manyani amphibolites, which form the wallrocks to the Kotongweni tonalite gneiss and the Mkondene diorite. The ultramafic Sithilo complex is part of the Evuleka ultramafic suite. Numerous additional ultramafic bodies included in this unit are too small to be indicated at this scale. Similarly, granitic dykes and sills of the Wosi granitoid suite, though numerous and widespread throughout the Tugela, Mandleni and Madidima tectonostratigraphic packages, are too small to be shown here.

Mesoproterozoic oceanic arc (Arima *et al.*, 2001; Johnston *et al.*, 1998).

Four additional major plutonic bodies, the mafic/ultramafic layered Tugela Rand and Macala complexes, the Mkondene diorite and the Dimane granite, are recognized in the TTP. The close spatial relationship between the Tugela Rand complex, and the Mkondene diorite and Dimane granite intrusions is thought to indicate that these plutonic bodies share a genetic link. Numerous serpentinite and talc lenses are presumed to define imbricate thrust faults (Harmer, 1979; Matthews, 1959).

2.2. Mandleni tectonostratigraphic packages

The Mandleni tectonostratigraphic package (MTP) sits structurally beneath the TTP. The bimodal Dondwana tectonite unit underlies most of the MTP and consists of tectonized and interfoliated schist and gneiss. Two main lithologies are recognized; amphibolite, covering 25% of the bedrock exposures, and leucocratic feldspathic gneiss, constituting the remaining 75% of the bedrock exposures. Contacts between these lithologies are sharp, paralleling the dominant planar fabric within the rocks. Banded grey tonalitic gneiss is rare. Rare discontinuous lenses of marble occur locally within
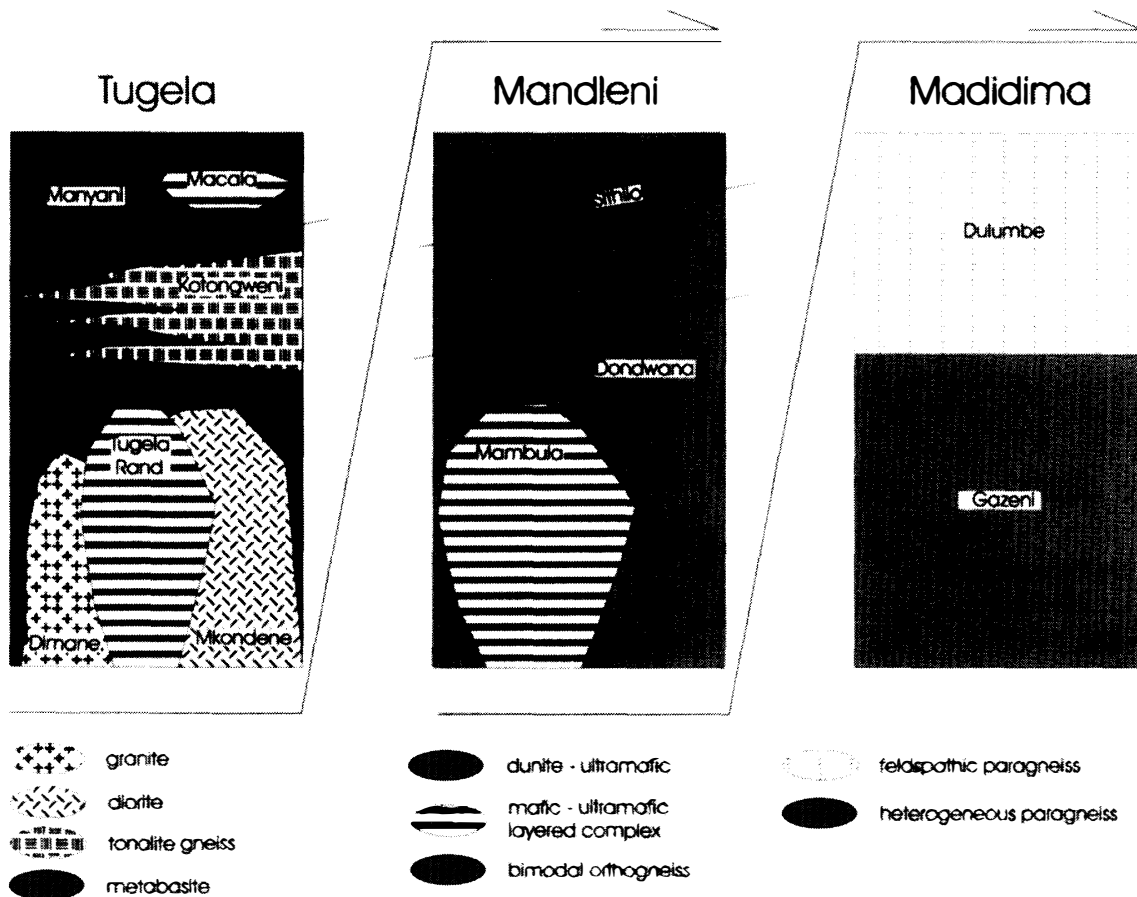
Fig. 3. Schematic cross section showing the stratigraphy of the Tugela, Mandleni and Madidima tectonostratigraphic packages. Not indicated here are intrusions of the Wosi granitoid suite, dykes, sills and plugs of which are present within all three tectonostratigraphic packages.

amphibolite. Geochemical studies (Arima *et al.*, 2001; Johnston *et al.*, 1998) have demonstrated that the feldspathic gneisses and metabasites are characterised by high abundances of Nb, Ti, LIL and HFS elements similar to ocean island basalts.

Two major igneous complexes, the ultramafic Sithilo, part of the Evuleka ultramafite suite, and the layered gabbroic Mambula complex, are recognized. The Sithilo complex is host to economic chromitite deposits (Wuth and Archer, 1986). The Evuleka ultramafite suite includes numerous small serpentinized lenses of harzburgite and talc. Together, the Sithilo complex and the harzburgitic lenses are interpreted as altered and sheared mantle or cumulates from the lower portion of an ophiolite (Johnston *et al.*, 2001; Matthews, 1959; Schulze-Hulbe, 1977). The Mambula complex consists of a heterogeneous array of gabbro, pyroxenite and massif anorthosite. It is host to sub-economic deposits of titaniferous magnetite (Reynolds, 1986).

2.3. Madidima tectonostratigraphic package

The structurally highest portion of the Madidima tectonostratigraphic package (MDTP), which crops out immediately beneath strata included in the MTP, consists of a

thick succession of homogeneous leucocratic biotite feldspathic gneiss, referred to as the Dulumbe paragneiss (Johnston *et al.*, 2001). The gneiss passes gradationally downward into a heterogeneous succession of garnetiferous biotite and muscovite biotite schist and gneiss, calc-silicate gneiss, minor amphibolite and marble, referred to as the Gazeni metasedimentary sequence (Matthews and Charlesworth, 1981). Although previously mapped as an orthogneiss (Matthews and Charlesworth, 1981), the gradational contact with the underlying metasedimentary sequence suggests that feldspathic gneiss may have been derived from an immature feldspathic sediment, for instance a greywacke or feldspathic sandstone.

2.4. Wosi granitoid suite

Significant volumes of leucocratic granitoid sheets and dykes intrude the TTP, MTP and the MDTP, locally accounting for as much as 40% of the outcrop. These granitoids consist of massive to weakly foliated grey quartz monzonite and granite, with lesser amounts of muscovite granite and quartz syenite. They most commonly occur as concordant, 5–100 cm thick sills emplaced parallel to foliation in the enclosing wall rocks; thicker (10–20 m) concordant sheets are less common. Locally the sills transect foliation in the enclosing rocks, are connected to adjacent sills by cross-cutting dykes, exhibit irregular (non-planar) margins, intrude along the axial surfaces of folds and thrust faults, and include xenoliths of foliated wall rock.

3. Structural geology and metamorphism

Primary structures in rocks of the TTP, MTP and MDTP have been largely obliterated during post-depositional metamorphism and deformation. Three distinct planar fabrics (S_{1-3}) developed during progressive north-verging deformation (D_{1-3}) and syn-kinematic metamorphism and are interpreted to have developed during two collisional events, including overthrusting of the Kaapvaal craton. A fourth fabric (S_4) provides a record of syn-kinematic retrogressive metamorphism during post-accretionary sinistral strike-slip displacement of the Natal tectonic belt (Johnston *et al.*, 2001).

A planar fabric (S_1) attributable to the oldest recognized deformation event (D_1) has been largely overprinted during subsequent deformation. Because of overprinting during subsequent tectonism, little is known about this early event. Fabric in the Kotongweni tonalite gneiss is thought to be in part S_1, suggesting that D_1 tectonism post-dated and is younger than the protolith of the Kotongweni tonalite gneiss.

The dominant S_2 planar fabric, a penetrative axial planar fabric, parallels lithological contacts and is defined by colour and compositional banding, and by parallelism of coarsely crystalline mineral grains. Rare detached isoclinal intrafolial folds of S_1 indicate that S_2 developed in response to isoclinal folding and transposition of older contacts (D_2). Folds and map-scale nappes, back rotation of boudins, and extensional shear bands indicate that D_2 was characterized ductile deformation during top-to-the-north shearing. Syn-kinematic high pressure (Opx-absent, P>9 kbar) granulite facies metamorphism coeval with D_2 gave rise to migmatized metabasite and grey gneiss, brown hornblende + plagioclase + quartz + diopside ± garnet amphibolites, and perthitic K feldspar + antiperthitic plagioclase + quartz + biotite ± hornblende ± garnet feldspathic gneiss.

Intrusion of plutonic bodies, including the mafic/ultramafic layered Tugela Rand and Mambula complexes, and the Mkondene diorite, is thought to have occurred late during the D_2 thermotectonic event. The Mambula complex experienced high pressure upper amphibolite metamorphism (Reynolds, 1986), consistent with intrusion late during D_2 metamorphism. All three plutonic bodies lack a through-going penetrative fabric. However, a strongly developed fabric that parallels the S_2 fabric in the enclosing wall rocks is locally developed along the margins of these plutonic bodies, and fabric development is present within dykes and sills attributable to these intrusions.

A D_3 tectonic event is indicated by folding and faulting of the S_2 fabric. Folds are highly asymmetric, being characterized by short steep north limbs and long shallowly dipping south limbs, and verge to the north. The lower limbs and cores of these folds are commonly broken by north-verging brittle-ductile shear zones and thrust faults. Syn-kinematic lower amphibolite-facies metamorphism resulted in retrogressive overprinting of much of the S_2 mineral parageneses by blue-green hornblende + plagioclase + quartz ± garnet amphibolites, and the growth of muscovite in the feldspathic rocks. This S_3 fabric parallels S_2 in the long limbs of the F_3 folds (most places) occurring at an angle to S_2 in fold hinges and locally along fold limbs. Recrystallization did not obliterate the older S_2 migmatitic texture, giving rise to migmatites whose lower amphibolite grade mineral paragenesis is inconsistent with the migmatitic appearence of the rocks. Plagioclase ± biotite mantles on garnet developed at this time and are attributable to garnet breakdown during isothermal exhumation.

Discontinuous lenses of ultramafic rocks (components of the Evuleka ultramafite suite) lie along the contacts between the tectonostratigraphic packages, are tectonically interleaved within the packages, lack evidence of high pressure – temperature metamorphism, and are interpreted to post-date D_2 deformation and metamorphism. The ultramafic rocks occur as discontinuous lenses that define linear belts coincident with structural and stratigraphic breaks, including the contacts between the tectonostratigraphic packages, and are interpreted to lie along and define major faults. These faults appear to be north-verging, are characterized by the same relationships to their foot- and hangingwall rocks as the D_3 thrusts described above, and are interpreted as map-scale D_3 thrust faults.

Voluminous granitoid magmatism of the Wosi granitoid suite, began prior to, and was in part coeval with folding and faulting of S_2, and the development of S_3. Sheets, dykes and plugs of leucocratic granite and quartz monzonite typically lack a penetrative fabric, truncate, and post-date S_2. Granitic sills intruded parallel to the dominant S_2 fabric and are, together with their gneissic wallrocks, commonly deformed within F_3 folds. North-verging D_3 thrust faults locally truncate and offset these sills. However, discordant granitic dykes cutting across F_3 folds and plugging D_3 thrust faults are also present, and point to continued magmatism after the cessation of D_3 deformation.

Broad open, south-plunging, folds of S_{1-3}, the coeval development of a heterogeneous array of narrow brittle-ductile shear zones and faults, and local (shear zone related) greenschist facies metamorphism characterize the final regional deformation event, D_4, recorded in the area. Recrystallization during retrogressive metamorphism resulted in the local development of a schistosity (S_4) defined by weakly aligned biotite + chlorite ± muscovite flakes. Significant retrogressive metamorphism within the shear

zones gave rise to actinolite, epidote, chlorite, prehnite and pumpellyite and sericite alteration of hornblende and feldspar grains. The orientation of the broad F_4 folds and related shear zones are consistent with folding during sinistral shearing of the Tugela terrane. It seems likely that the northern margin of the Tugela terrane is a sinistral strike-slip fault, and that accretion of the Tugela terrane occurred well to the west (present day coordinates) of the present location of the Tugela terrane.

4. Geochronology

4.1. Previous studies

Previous geochronological data from the Tugela terrane and plutonic rocks that intrude it are summarized in Table 1. Several broad conclusions can be drawn from this data.

1) Ar-Ar cooling ages on hornblende indicate final cooling and exhumation of the Tugela terrane occurred between 1135 and 1077 Ma. Thus regional penetrative deformation and metamorphism affecting the Tugela terrane pre-dates 1135 Ma.

2) Rb-Sr isotopic systems have experienced post-crystallization disturbances, resulting in large errors on age determinations, and rendering much of this data difficult to interpret.

3) A Sm-Nd mineral isochron age for the Tugela Rand complex of 1189±14 Ma (A. Wilson, written communication in South African Committee for Stratigraphy, 1990) may indicate intrusion at around 1190 Ma. However, data for this study have yet to be published.

4.2. Analytical techniques

U-Pb zircon age determinations were obtained from samples of 5 different units (Table 2): (1) leucocratic biotite feldspathic gneiss of the Dulumbe paragneiss from the MDTP; (2) garnet hornblende tonalite gneiss of the Kotongweni tonalite gneiss from the TTP; (3) hypersthene biotite diorite of the Mkondene diorite from the TTP; (4) pegmatitic anorthosite from massif anorthosite of the Mambula complex, part of the MTP; and (5) leucocratic quartz monzonite of the Wosi granitoid suite, a unit that overlaps all three tectonostratigraphic packages. Sample sizes varied from 10 to 25 kg. Heavy-mineral concentrates were prepared from individual samples using standard Wilfley table, heavy liquid, and magnetic separation techniques. Some of the U-Pb analyses were done using the SHRIMP I Facility at the Australian National University (ANU), Canberra; and some were done at the Radiogenic Isotope Facility (RIF) at the University of Alberta. Here we report data only from samples of the Dulumbe paragneiss and the Kotongweni tonalite gneiss. However, we do present preliminary age determinations (without supporting data) for the other samples, which are currently still in the process of being analyzed.

At the University of Alberta, isolation of U and Pb from a dissolved sample with a mixed $^{205}Pb/^{235}U$ tracer solution was carried out in the chemistry laboratory in the RIF following established anion exchange chromatography procedures (Krogh, 1973). The total analytical blank levels during this study were 6–9 pg for Pb and <2 pg for U. The purified Pb and U were loaded together onto precleaned zone refined Re ribbon using the

Table 1. Results of previous geochronological investigations of the Tugela terrane.

Thrust Sheet	Unit	Isotopic System	Age determination	Reference	Comment
Tugela	Mkondene Diorite (deformed)	Rb-Sr	955 ± 53 Ma	Barton, 1983	sampled a strained, gneissic zone within the pluton; regression of 11 samples
	Mkondene Diorite	Rb-Sr	1169 ± 142 Ma	Barton, 1983	sampled undeformed diorite; regression of 9 samples
	Tugela Rand layered intrusion	Sm-Nd	1189 ± 14 Ma	Wilson, 1990[1]	a mineral isochron age
	Dimane Granite	Rb-Sr	1202 ± 84 Ma	Barton, 1983	regression of 4 samples
	Tuma Formation[2]	Rb-Sr	1224 ± 88 Ma	Barton, 1983	regression of 11 samples
	Tuma Formation[2]	Rb-Sr	1218 ± 96 Ma	Harmer, 1979	regression of 7 samples
Mandleni	Dondwana feldspathic gneiss[3]	Rb-Sr	1093 ± 108 Ma	Barton, 1983	regression of 10 samples
	Dondwana feldspathic gneiss[3]	U-Pb Titanite[4]	~1080 Ma	Barton, 1983	a metamorphic cooling age?
	Dondwana feldspathic gneiss[3]	U-Pb Zircon[4]	~1152 Ma	Barton, 1983	average of 3 $^{207}Pb/^{206}Pb$ ages for highly discordant bulk zircon separates
	Dondwana amphibolite[5]	Ar-Ar	1135± 9 Ma	Thomas et al., 1996	analysis of a hornblende separate
	Dondwana amphibolite[6]	Ar-Ar	1077 ± 11 Ma	Thomas et al., 1996	analysis of a hornblende separate
Madidima	Gazeni amphibolite[7]	Ar-Ar	1080 ± 6 Ma 1112 ± 6 Ma	Thomas et al., 1996	analyses of hornblende separates
Nkomo	Bull's Run Syenite	U-Pb zircon[2]	1140 ± 35 Ma	Nicolaysen & Burger, 1965	A $^{207}Pb/^{206}Pb$ age
	Ngoye Granite	Rb-Sr	1067 ± 20 Ma	Barton, 1983	regression of 5 samples
	Ngoye Granite	U-Pb zircon[2]	~1041 Ma	Barton, 1983	average of 3 $^{207}Pb/^{206}Pb$ ages for highly discordant bulk zircon separates
	Khomo Formation	Rb-Sr	1181 ± 126 Ma	Barton, 1983	regression of 10 samples
	Halambu Gneiss	Rb-Sr	780 ± 672 Ma	Barton, 1983	regression of 5 samples; very large scatter of data
	Halambu Gneiss	U-Pb zircon[2]	~1119 Ma	Barton, 1983	average of 3 $^{207}Pb/^{206}Pb$ ages for highly discordant bulk zircon separates

1 - written communication in South African Committee for Stratigraphy, 1990: 2 – Tuma Formation consists of interlayered sedimentary rocks and metabasalt that forms a separate thrust sheet near the base of the TTP; 3 – Referred to as Dondwana Formation in oroginal studies; 4 - bulk mineral separates; 5 – Referred to as the Wosi formation in the original studies; 6 – Referred to as the Tholwane amphibolite in the original studies; 7 – Referred to as Madidima amphibolite in original study.

Table 2. Sample list with locations and analytical technique applied.

Sample	Unit	Sample S. Lat.	Location W. Long.	Description	Analytical Technique	Zircons
STJ 97T 38	Madidima gneiss	28.872	30.733	Leucocratic biotite feldspathic gneiss	SHRIMP	heterogeneous array of anhedral zoned grains
STJ 96T 4	Kotongweni gneiss	28.773	30.900	Garnet hornblende tonalite gneiss	SHRIMP	rust coloured euhedral grains
STJ 96T 1	Mkondene pluton	28.847	30.867	Hypersthene biotite diorite	TIMS	Abundant euhedral cloudy grains
STJ 98T 5	Mambula magmatic complex	28.975	31.055	Pegmatitic pyroxene anorthosite	TIMS	large clear euhedral grain fragments
AB 99 Z (A-C)	Wosi granitoid suite	31. 074	28.833	Leucocratic quartz monzonite	SHRIMP	

Si-gel technique (Cameron *et al.*, 1969), and their isotopic composition was determined on a VG354 mass spectrometer operating in single-collector mode. Isotopic ratios measured using a Daly photomultiplier detector (typically the $^{205}Pb/^{204}Pb$ and $^{238}U/^{235}U$ ratios) were corrected using an empirically derived conversion factor of +1.3‰/amu for Pb and +1.5‰/amu for U. All isotopic ratios were corrected for mass discrimination (0.88‰/amu Pb; 1.55‰/amu U) based on repeated analyses of the NIST SRM981 Pb and U500 standards. The 1σ analytical uncertainties reported in the data tables were calculated using an in-house numerical error propagation routine.

At ANU, zircons were mounted in epoxy together with chips of the Research School of Earth Sciences (RSES) zircon standards SL 13 and AS3 of the Duluth Complex gabbroic anorthosite (Paces and Miller, 1989). All unknown and standard zircons were polished to approximately half their thickness in order to expose any internal structure. Microphotographs using reflected and transmitted light were used to select target areas, and these were subsequently checked using SEM cathodoluminescence imaging. The U-Th-Pb data were reduced in a manner similar to that described by Williams and Claesson (1987) and Compston *et al.* (1992). The Pb/U ratios have been normalized to a value of 0.1859 for the $^{206*}Pb/^{238}U$ ratio for the AS3 standard, equivalent to an age of 1099.1 Ma. U-Pb ages were calculated using the decay constants recommended by Steiger and Jäger (1977), and have been corrected for common Pb using the directly measured ^{204}Pb abundances and the appropriate common Pb compositions according to the Cumming and Richards (1975) model. Uncertainties in the isotopic ratios and ages listed in the data tables (Tables 3 and 4) and plotted in the figures are one sigma. Where data are pooled to calculate weighted mean or concordia intercept ages using the statistical package Isoplot/Ex (Ludwig, 1998), uncertainties are reported with 95% confidence limits.

4.3. Analytical results

4.3.1. Dulumbe paragneiss (MDTP)

The MDTP is the lowest structural unit sampled in this study, and has been interpreted as consisting of parauthochthonous strata that originated between the far-travelled oceanic rocks that comprise the TTP, and the Archaean Kaapvaal craton

exposed to the north of the Tugela terrane. The feldspathic Dulumbe paragneiss is interpreted as having been derived from an immature clastic sediment. U-Pb zircon age determinations (1) provide a test of the interpreted sedimentary origin of the gneiss, (2) place constraints on the age of the source rocks being eroded to produce the sedimentary protolith, and (3) limit the age of the sedimentary sequence.

The heterogeneous array of zircons from the sample are not well preserved. The lack of a single homogeneous population supports interpretation of the gneiss as a metasedimentary rock. The grains are generally anhedral, darkly coloured and translucent, with some showing irregular resorption and possible secondary growth around the edges. Cathodoluminescence images are generally dark with few original magmatic textures preserved. Most grains, however, have brightly luminescent margins and intragranular patches. The overall morphology of these patches suggests that they represent metamorphic recrystallization or growth (Fig. 4).

The heterogeneous age pattern produced by the SHRIMP U-Pb analyses (Table 3) reinforces interpretation of the rock as a metasediment characterized by detrital zircons. Severe discordance of many of the data points (Fig. 5) does introduce further complexities into the U-Pb age spectrum. The more concordant data points suggest derivation from a number of sources with an age range spanning about 100 m.y. The oldest grain gives a $^{207}Pb/^{206}Pb$ age of 1289±14 Ma (2σ). Four analyses of the highly luminescent areas, interpreted as metamorphic growth or reworked zircon, give a weighted mean $^{207}Pb/^{206}Pb$ age of 1182±19 Ma (MSWD=0.39, probability=0.76) (Fig. 6),

Fig. 4.   Cathodoluminescence image of sectioned zircons from sample STJ97T38 (Dulumbe paragneiss). Areas analysed are shown (see Table 3 for data). Note the brightly luminescent rims and intragranular patches, interpreted as metamorphic zircon.

Table 3.   Summary of SHRIMP U-Pb analytical data for sample STJ97T38 (Dulumbe paragneiss).

Grain spot	U (ppm)	Th (ppm)	Th/U	Pb* (ppm)	$^{204}Pb/$ ^{206}Pb	f_{206} %	$^{206}Pb/$ ^{238}U	±	$^{207}Pb/$ ^{235}U	±	$^{207}Pb/$ ^{206}Pb	±	$^{206}Pb/$ ^{238}U	±	$^{207}Pb/$ ^{235}U	±	$^{207}Pb/$ ^{206}Pb	±	Conc. %
1.1m	119	70	0.59	11	0.000490	0.82	0.0913	0.0015	0.996	0.037	0.0791	0.0025	563	9	702	19	1176	63	48
2.1	269	224	0.83	66	0.000435	0.73	0.2128	0.0029	2.405	0.042	0.0820	0.0008	1244	15	1244	13	1245	19	100
3.1	496	205	0.41	99	0.000052	0.09	0.1975	0.0024	2.150	0.030	0.0790	0.0004	1162	13	1165	10	1171	10	99
4.1	227	60	0.26	42	0.000049	0.08	0.1862	0.0024	2.052	0.037	0.0800	0.0009	1101	13	1133	12	1196	22	92
5.1	380	268	0.70	84	0.000015	0.03	0.1973	0.0027	2.225	0.034	0.0818	0.0005	1161	15	1189	11	1241	11	94
6.1	1131	354	0.31	142	0.000065	0.11	0.1246	0.0017	1.313	0.020	0.0765	0.0004	757	10	852	9	1107	10	68
7.1	590	732	1.24	151	0.000050	0.08	0.2050	0.0026	2.341	0.033	0.0828	0.0003	1202	14	1225	10	1265	8	95
7.2	376	387	1.03	89	0.000034	0.06	0.1989	0.0050	2.294	0.059	0.0836	0.0004	1170	27	1210	18	1284	9	91
8.1	725	287	0.40	133	0.000071	0.12	0.1730	0.0023	1.889	0.028	0.0792	0.0004	1029	12	1077	10	1177	11	87
9.1	1210	2593	2.14	453	0.000055	0.09	0.2592	0.0033	3.011	0.041	0.0842	0.0003	1486	17	1410	10	1298	7	115
10.1	1874	678	0.36	213	0.000119	0.20	0.1112	0.0021	1.160	0.024	0.0757	0.0005	680	12	782	11	1086	12	63
11.1	2413	181	0.07	208	0.000560	0.94	0.0875	0.0011	0.891	0.015	0.0738	0.0007	541	7	647	8	1036	20	52
12.1	945	1304	1.38	243	0.000077	0.13	0.2042	0.0026	2.307	0.031	0.0820	0.0003	1198	14	1215	10	1244	7	96
13.1	880	227	0.26	185	0.000010	0.02	0.2000	0.0030	2.176	0.034	0.079	0.0003	1175	16	1173	11	1170	7	101
14.1	571	417	0.73	143	0.000061	0.10	0.2180	0.0032	2.442	0.038	0.0812	0.0004	1272	17	1255	11	1227	9	104
15.1	707	479	0.68	107	0.000142	0.24	0.1377	0.0019	1.509	0.023	0.0795	0.0004	832	11	934	9	1183	9	70
16.1m	765	450	0.59	129	0.000279	0.47	0.1547	0.0024	1.683	0.035	0.0789	0.0010	927	13	1002	13	1169	24	79
17.1	1199	275	0.23	156	0.000094	0.16	0.1311	0.0019	1.405	0.022	0.0778	0.0004	794	11	891	9	1141	9	70
18.1	519	376	0.72	103	0.000071	0.12	0.1749	0.0025	1.944	0.031	0.0806	0.0004	1039	14	1096	11	1212	10	86
19.1	452	488	1.08	111	0.000014	0.02	0.2045	0.0030	2.338	0.036	0.0829	0.0003	1199	16	1224	11	1268	6	95
20.1m	415	146	0.35	83	0.000010	0.02	0.1951	0.0033	2.145	0.040	0.0797	0.0005	1149	18	1163	13	1190	12	97
21.1m	209	50	0.24	29	0.000112	0.19	0.1375	0.0022	1.496	0.030	0.0789	0.0008	831	13	929	12	1170	20	71
22.1	351	213	0.61	82	0.000019	0.03	0.2129	0.0037	2.433	0.046	0.0829	0.0004	1244	20	1253	14	1267	10	98
23.1	1345	903	0.67	158	0.000081	0.14	0.1101	0.0016	1.141	0.018	0.0752	0.0004	673	9	773	9	1073	11	63
24.1	270	244	0.90	69	0.000000	0.00	0.2210	0.0033	2.506	0.042	0.0822	0.0005	1287	17	1274	12	1251	12	103

Notes :   Uncertainties given at the one σ level; f206 % denotes the percentage of 206Pb that is common Pb.
For % Conc., 100% denotes a concordant analysis; m = metamorphic zircon
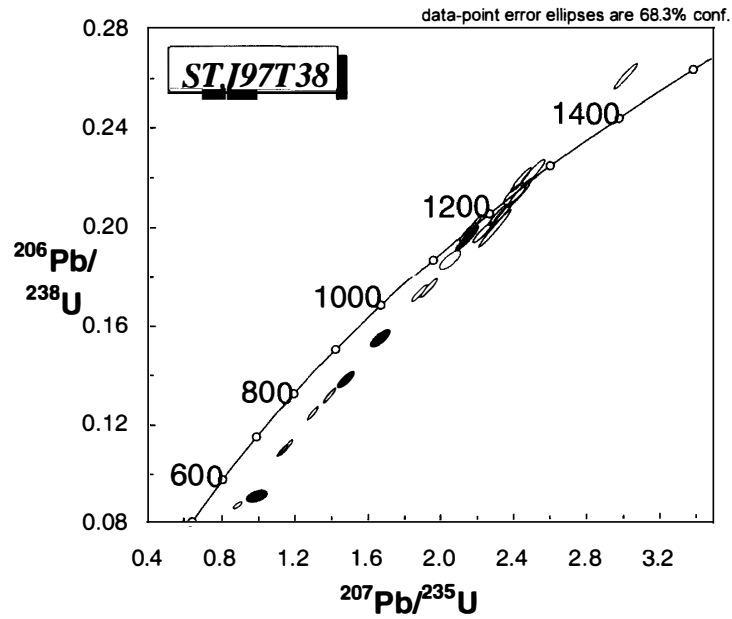
Fig. 5. U-Pb concordia diagram showing SHRIMP data for zircons from sample ST.I97T38 (Dulumbe paragneiss). The grey-shaded error boxes represent the data for the metamorphic rims.
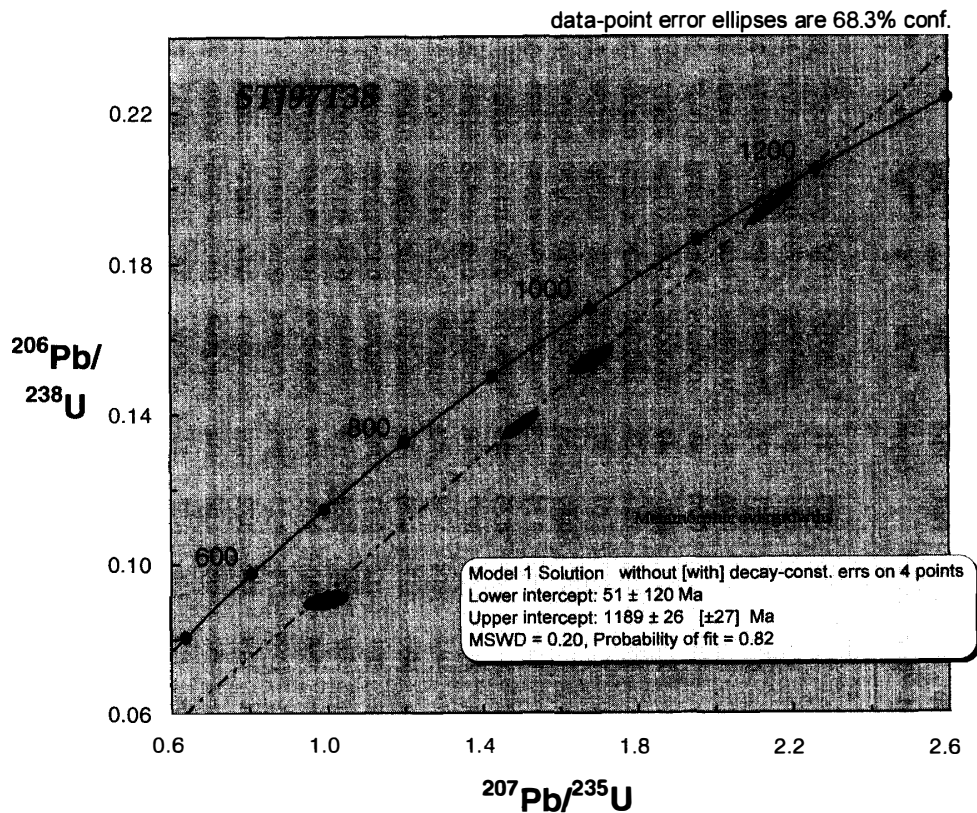
Fig. 6. U-Pb concordia diagram showing SHRIMP data for only metamorphic zircon from sample STJ97T38 (Dulumbe paragneiss).

but it must be borne in mind that three of these analyses are highly discordant. Regression of these same data points gives an upper intercept age of 1189±26 Ma (95% confidence limits) and a recent lower intercept age of 51±120 Ma (MSWD=0.2, probability=0.82). This demonstrates that Pb-loss is recent, and these rocks suffered no significant post-crystallization intermediate Pb-loss. In order to determine the different provenance ages for the zircons, it was considered appropriate to use only the more concordant data points for mixture modeling (Sambridge and Compston, 1994) calculations. From the >90% concordant U-Pb data three $^{207}Pb/^{206}Pb$ age groups are indicated, with uncertainties quoted as 95% confidence limits. These are: (1) 1276±10 Ma (38% of the data); (2) 1240±10 Ma (35% of the data); and (3) 1175±9 Ma (27% of the data). The youngest age group is within uncertainty of the age determined for the metamorphic phase and is interpreted to represent the age of syn-metamorphic Pb-loss from the inherited zircons, the growth of metamorphic zircon rims on existing grains, and the recrystallization of pre-existing zircons. This age places a lower age limit of deposition of the original sediment. The older zircons represent the maximum age of deposition.

4.3.2. Kotongweni tonalite gneiss (TTP)

The Kotongweni tonalite gneiss is thought to be the oldest plutonic element identified in the Tugela terrane. It predates D_1 tectonism and, together with its related metabasitic wallrocks forms part of an oceanic magmatic arc. Therefore the gneiss provides us with a chance to determine the age of this magmatic arc, and to place a maximum age constraint on D_1 tectonism.

The sample yielded zircons of variable shape, form, colour and size. One sub-population comprised relatively large (200–250 μm) clear, colourless, and multi-facetted oblate crystals. Cathodoluminescence imaging of these grains shows compositional and sector zoning. The smaller zircons (generally about 100 μm in size) tend to be anhedral, brown and give darker cathodoluminescence images indicative of higher uranium contents. Cathodoluminescence imaging also shows that all grains have a narrow rim of low-U metamorphic zircon.

Twenty-six analyses were performed on twenty different zircons in an attempt at establishing a magmatic age for this sample, with low-U grains yielding relatively low precision (Table 4). Despite the apparent heterogeneity in the chemistry and morphology of the zircons from the tonalitic gneiss, all analyses cluster around concordia (Fig. 7) and combine to give a weighted mean $^{207}Pb/^{206}Pb$ age of 1209±5 Ma (MSWD=1.04; probability=0.41).

4.3.3. Mkondene diorite (TTP) and massif anorthosite of the Mambula complex (MTP)

These intrusive bodies were emplaced into volcanic and sedimentary rocks of the Tugela and Mandleni tectonostratigraphic packages, respectively, post-date D_1 deformation, and were emplaced late during the syn-kinematic high pressure-high temperature D_2 event. The pre-date folding and faulting attributable to the D_3 and D_4 tectonic events. Therefore they provide a minimum age constraint on the age of the protoliths of the Manyani and Dondwana units, a minimum age constraint on D_1 tectonism, a direct determinaton of the age of D_2 tectonism, and a maximum age constraint on D_3 tectonism.

Only preliminary results are provided as U-Pb analyses are ongoing. The $^{207}Pb/^{206}Pb$

Table 4.   Summary of SHRIMP U-Pb analytical data for sample STJ96T4 (Kotongweni tonalite gneiss).

Grain. spot	U (ppm)	Th (ppm)	Th/U	Pb* (ppm)	$^{204}Pb/^{206}Pb$	f_{206} %	Radiogenic Ratios $^{206}Pb/^{238}U$	±	$^{207}Pb/^{235}U$	±	$^{207}Pb/^{206}Pb$	±	Ages (in Ma) $^{206}Pb/^{238}U$	±	$^{207}Pb/^{235}U$	±	$^{207}Pb/^{206}Pb$	±	Conc. %
1.1	220	45	0.2	46	0.000057	0.10	0.2148	0.0035	2.372	0.043	0.0801	0.0005	1254	18	1234	13	1199	13	105
1.2	171	32	0.19	34	0.000073	0.12	0.2071	0.0027	2.283	0.044	0.0799	0.0010	1213	15	1207	14	1195	25	102
2.1	911	790	0.87	234	0.000025	0.04	0.2247	0.0032	2.514	0.037	0.0812	0.0003	1306	17	1276	11	1225	6	107
2.2	240	109	0.45	53	0.000064	0.11	0.2133	0.0025	2.367	0.036	0.0805	0.0007	1246	13	1233	11	1209	17	103
3.1	231	34	0.15	48	0.000034	0.06	0.215	0.0032	2.379	0.040	0.0803	0.0005	1256	17	1236	12	1203	12	104
4.1	61	11	0.18	12	0.000206	0.35	0.2075	0.0048	2.318	0.084	0.0811	0.0020	1215	26	1218	26	1223	50	99
4.2	65	10	0.15	13	0.000010	0.02	0.2124	0.0044	2.364	0.056	0.0807	0.0007	1241	24	1232	27	1215	17	102
5.1	37	7	0.19	8	0.000519	0.87	0.2121	0.0044	2.274	0.088	0.0778	0.0024	1240	23	1204	28	1141	62	109
6.1	57	15	0.27	12	0.000510	0.85	0.2059	0.0039	2.214	0.078	0.0780	0.0022	1207	21	1185	25	1146	56	105
7.1	271	111	0.41	59	0.000010	0.02	0.2107	0.0032	2.359	0.040	0.0812	0.0005	1232	17	1230	12	1227	12	101
8.1	130	28	0.22	26	0.000135	0.23	0.2063	0.0034	2.244	0.054	0.0789	0.0012	1209	18	1195	17	1170	31	103
9.1	149	45	0.3	32	0.000073	0.12	0.2102	0.0037	2.305	0.047	0.0795	0.0007	1230	19	1214	15	1185	18	104
10.1	208	95	0.46	47	0.000103	0.17	0.2163	0.0036	2.378	0.048	0.0797	0.0008	1262	19	1236	14	1190	19	106
11.1	87	19	0.22	18	0.000299	0.50	0.2074	0.0036	2.264	0.062	0.0792	0.0015	1215	19	1201	19	1177	38	103
11.2	36	5	0.13	8	0.000339	0.57	0.2176	0.0046	2.467	0.087	0.0823	0.0021	1269	24	1263	26	1252	52	101
12.1	426	116	0.27	90	0.000689	1.15	0.212	0.0031	2.332	0.045	0.0798	0.0008	1240	17	1222	14	1191	21	104
12.2	592	176	0.3	121	0.000624	1.04	0.2034	0.0024	2.273	0.036	0.0810	0.0008	1195	13	1204	11	1222	19	98
13.1	40	6	0.15	8	0.000144	0.24	0.2099	0.0042	2.361	0.061	0.0816	0.0012	1228	22	1231	19	1236	28	99
14.1	29	8	0.26	6	0.000417	0.70	0.2074	0.0039	2.263	0.077	0.0791	0.0021	1215	21	1201	24	1175	52	103
14.2	39	6	0.15	8	0.000101	0.17	0.2211	0.0043	2.406	0.062	0.0789	0.0012	1288	23	1244	19	1170	30	110
15.1	953	440	0.46	212	0.000020	0.03	0.2131	0.0023	2.361	0.028	0.0804	0.0003	1245	12	1234	8	1206	8	103
16.1	84	17	0.21	17	0.000032	0.05	0.2122	0.0035	2.348	0.048	0.0803	0.0008	1240	19	1227	15	1204	20	103
17.1	17	3	0.21	4	0.000082	0.14	0.2147	0.0053	2.392	0.083	0.0808	0.0017	1254	28	1240	25	1217	43	103
18.1	468	130	0.28	97	0.000037	0.06	0.2063	0.0029	2.293	0.035	0.0806	0.0003	1209	16	1210	11	1212	8	100
19.1	681	264	0.39	131	0.000018	0.03	0.1872	0.0027	2.072	0.031	0.0803	0.0002	1106	14	1140	10	1204	6	92
20.1	459	123	0.27	98	0.000010	0.02	0.2142	0.0031	2.361	0.037	0.0800	0.0004	1251	16	1231	11	1196	9	105

Notes: Uncertainties and symbols as in Table 3.
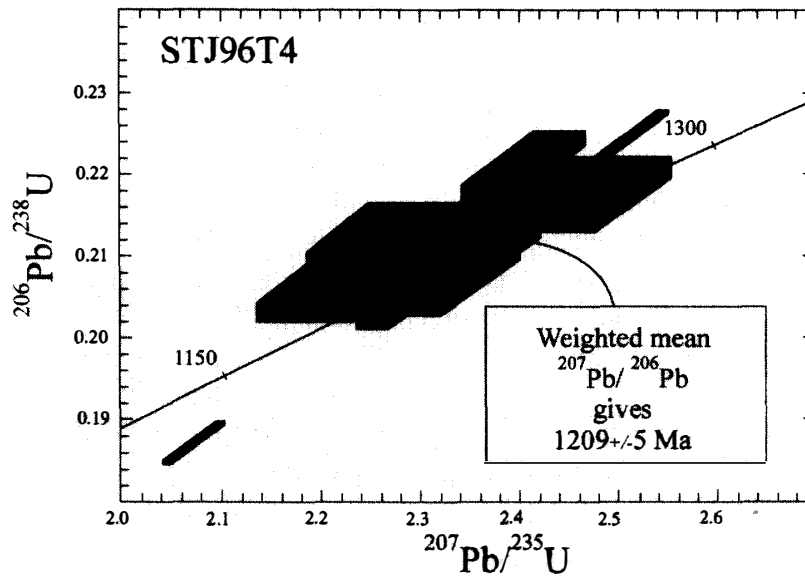
Fig. 7. *U-Pb concordia diagram showing the SHRIMP data for zircons from sample STJ96T4 (Kotongweni tonalite gneiss). The weighted mean $^{207}Pb/^{206}Pb$ age shown was calculated from all twenty-six analyses. The concordia curve is calibrated in M.y.*

age for a 10 zircon grain fraction from the sample of the Mkondene diorite is 1168 Ma (1.9% discordant). A $^{207}Pb/^{206}Pb$ age for a similar sized fraction from the sample of massif anorthosite from the Mambula complex is 1157 Ma (3.1% discordant). The two fractions lie along and define a discordia line with an upper intercept of 1181 Ma and a lower intercept of 540 Ma. We interpret these results to indicate intrusion and crystallization of these plutons at about 1181 Ma. The Early Paleozoic lower intercept is poorly defined and no significance can, at this point, be ascribed to this date. It does suggest that both intrusive bodies were affected by a tectonic or thermal event that resulted in the loss of radiogenic Pb from zircon sometime in the Neoproterozoic—early Paleozoic.

4.3.4. Wosi granitoid suite (overlapping magmatic suite)

Plugs, sheets, and dykes of this magmatic suite intrude all three tectonostratigraphic packages and constitute an overlap assemblage. In addition they cross-cut, post-date and provide a minimum age constraint on the S_2 fabric, and intruded during and provide a direct determination of the age of D_3 tectonism. Preliminary results of SHRIMP analyses indicate a crystallization age of 1155±1 Ma.

5. Discussion and conclusions

Our data places important constraints on the origin and early evolution of the Tugela terrane, and provide evidence of an oceanic origin for the terrane, far removed from any influence by the Kaapvaal craton. Metasedimentary rocks of the MDTP, the structurally lowest and presumabley most autochthonous of the tectonostratigraphic packages sampled as part of this study, are characterized by detrital zircons with a maximum age of 1276± 10 Ma. This age (1) is the oldest age yet reported from the entire Natal belt, (2)

provides a maximum age constraint for the sedimentary protoliths of the metamorphic rocks that make up the MDTP, and (3) limit the possible source terrain of these meta-clastic rocks. It is apparent that the adjacent Kaapvaal craton, which is characterized by the Meso-archaean Pongolo Group, lacks Proterozoic rocks and is not the source of these sediments. This would suggest that the Tugela terrane, was far removed from the Kaapvaal craton during deposition of the sedimentary protolith of the Dulumbe paragneiss. Because these detrital zircons are only slightly older than the oldest magmatic component of the Tugela terrane, it may be that the sediments are autolithic, and the source of the sediments is to be found within the Tugela terrane, as opposed to a distal cratonic source. Thus, interpretation of the structurally lowermost components of the Tugela terrane as being parautochthonous, is probably incorrect. Isotopic studies, to determine the extent to which the meta-clastic rocks of the MDTP were derived from erosion of an evolved or a juvenile source region, are necessary to test the autolithic source hypothesis.

The oceanic magmatic arc comprised by the Kotongweni tonalite gneiss and its metabasitic wall rocks, part of the TTP, was active at 1209±5 Ma, the age of the Kotongweni tonalite gneiss. The tonalite body predates, and therefore places a maximum age constraint on subsequent deformation and metamorphism of the Tugela terrane.

The Tugela terrane was subsequently deeply buried, metamorphosed and deformed. Metamorphic zircon (rims and recrystallized grains) from the Dulumbe paragneiss, interpreted to have crystallized during this tectonic event, limits peak metamorphism to 1175±9 Ma. The TTP and MTP are characterized by significant syn- to post-tectonic magmatism, including emplacement of the Tugela Rand complex, and the Mkondene diorite and Dimane granite intrusions in the TTP, and the Mambula complex in the MTP. Crystallization of the Tugela Rand complex and the Mkondene diorite in the TTP, and the Mambula complex in the MTP at about 1180 Ma is consistent with interpretation of these intrusions being syn- to late tectonic. These relationships suggests that tectonic burial post-dated 1209 Ma, the age of the protolith of the Kotongweni tonalite gneiss, but pre-dated 1180 Ma. The emplacement of layered mafic/ultramafic complexes, including massif anorthosite, subsequent to tectonic burial and crustal thickening, implies a genetic relationship between tectonism and magmatism. Further research is necessary to determine the nature of this link.

Significant granitoid magmatism attended the uplift, retrogressive metamorphism, and the northward obduction of the Tugela terrane onto the Kaapvaal craton. Obduction appears to have been facilitated by the collapse of a basin floored by oceanic crust, as indicated by the tectonic interleaving of alpine-type ultramafic rocks along thrust faults at this time. The age of obduction is constrained by the crystallization age of syn-tectonic granites to have occurred at about 1155±1 Ma. This is consistent with ^{40}Ar-^{39}Ar hornblende ages of 1135 to 1077 Ma from metabasites of the Tugela terrane (Thomas *et al.*, 1996). The association of voluminous granitic magmatism with obduction of the Tugela terrane may be attributable to decompressive melting during exhumation of the deeply buried terrane. Alternatively, magmatism may have developed in response to the subduction of the oceanic crust that separated the Tugela terrane from the Kaapvaal craton, and which is locally preserved along thrust sheets within the terrane. Isotopic and geochemical studies should be able to resolve which of these hypotheses is correct.

These results are consistent with interpretation of the Tugela terrane as a short-lived oceanic terrane that developed during the tectonic construction of Rodinia. The interval between initial basin development (post 1276±10 Ma) and final obduction (at about 1155±1 Ma), spans little more than 100 My. This interval saw the development of a robust magmatic arc, indicating subduction beneath the terrane, and subsequent collision, tectonic burial and high P–high T metamorphism. These findings place tight limits on tectonic models of the evolution of the Tugela terrane, and hopefully help clarify the role of the Kaapvaal craton and its marginal Mesoproterozoic orogenic belts in the construction of Rodinia.

Acknowledgments

References

Arima, M., Tani, K., Kawate, S. and Johnston, S.T. (2001): Geochemical characteristics and tectonic setting of metamorphosed rocks in the Tugela terrane, Natal belt, South Africa. Mem. Natl Inst. Polar Res., Spec. Issue, 55, 1–39.

Barton, E.S. (1983): The geochronology of the frontal zones of the Namaqua-Natal Mobile Belt. Ph.D. Thesis, University of the Witwatersrand, Johannesburg, 205 p.

Cameron, A.E., Smith, D.E. and Walker, R.L. (1969): Mass spectrometry of nanogram size quantities of lead. Anal. Chem., 41, 525–526.

Compston, W., Williams, I.S., Kirschvink, J.L., Zhang, Z. and Guogan, M.A. (1992): Zircon U-Pb ages for the Early Cambrian time scale. J. Geol. Soc. London, 149, 171–184.

Cumming, G.L. and Richards, J.R. (1975): Ore lead isotope ratios in a continuously changing earth. Earth Planet. Sci. Lett., 28, 155–171.

Harmer, R.E. (1979): Pre-Cape Geology of the Tugela valley north of Kranskop, Natal. Unpublished M.Sc. thesis, University of Natal, 234 p.

Hoffman, P.F. (1991): Did the breakout of Laurentia turn Gondwanaland inside-out? Science, 252, 1409–1412.

Johnston, S.T., Arima, M., Keiji, T., Kawate, S., Shiraishi, K., Kimura, J. and McCourt, S. (1998): The Kotongweni Tonalite, Tugela Terrane, Southeastern Africa: The plutonic root of a Grenvillian oceanic arc. Geological Society of America Annual Meeting 1998, Toronto, 259.

Johnston, S.T., McCourt, S., Bisnath, A. and Mitchell, A. (2001): The Tugela terrane Natal tectonic belt: Kibaran magmatism and tectonism along the south-east margin of the Kaapvaal craton. submitted to S. Afr. J. Geol.

Krogh, T.E. (1973): A low-contamination method for hydrothermal decomposition of zircon and extraction of U and Pb for isotopic age determinations. Geochim. Cosmochim. Acta, 37, 485–494.

Ludwig, K.R. (1998): Isoplot/Ex (version 1.00): A geochronological toolkit for Microsoft Excel. Pulbications of Berkeley Geochronological Centre, 1, 1–43.

Matthews, P.E. (1959): The metamorphism and tectonics of the pre-cape formations in the post-ntingwe thrust-belt, S.W. Zululand, Natal. Trans. Geol. Soc. S. Afr., **62**, 257–322.

Matthews, P.E. (1972): Possible Precambrian obduction and plate tectonics in southeastern Africa. Nature, **240**, 37–39.

Matthews, P.E. and Charlesworth, E.G. (1981): Northern margin of the Namaqua-Natal mobile belt in Natal, 1:140 000 scale geological map: Durban, South Africa, University of Natal.

Nicolaysen, L.O. and Burger, A.J. (1965): Note on an extensive zone of 1 000 -million-year old metamorphic and igneous rocks in South Africa. Science de la Terre, **10**, 497–576.

Paces, J.B. and Miller, J.D. (1989): Precise U-Pb ages of Duluth Complex and related mafic intrusions, Northeastern Minnesota: Geochronological insights to physical, petrogenic, and paleomagnetic and tectonomagmatic processes associated with the 1.1 Ga midcontinent rift system. J. Geophys. Res., **98B**, 13997–14013.

Reynolds, I.M. (1986): The mineralogy and petrography of some vanadium-bearing titaniferous iron ores of the Mambula complex, Zululand. Mineral Deposits of Southern Africa, ed. by C.R. Anhaeusser and S. Maske. Johannesberg, Geological Society of South Africa, Vol.2, 1695–1708.

Sambridge, M.S. and Compston, W. (1994): Mixture modeling of multi-component data sets with application to ion-probe zircon ages. Earth Planet. Sci. Lett., **128**, 373–390.

Schulze-Hulbe, A. (1977): A study of the structure and metamorphism of the rocks of the Tugela group exposed in the Mambula Mbongolwane area, Natal. Unpublished M.Sc. thesis, Univ. of Natal, 229 p.

Steiger, R.H. and Jäger, E. (1977): Subcommission on geochronology: convention on the use of decay constants in geo- and cosmochronology. Earth Planet. Sci. Lett., **36**, 359–362.

Thomas, R.J. (1989): A tale of two tectonic terranes. S. Afr. J. Geol., **92**, 306–321.

Thomas, R.J., Cornell, D.H. and Armstrong, R.A. (1999): Provenance age and metamorphic history of the Quha Formation, Natal Metamorphic Province: a U-Th-Pb zircon SHRIMP study. S. Afr. J. Geol., **102**, 83–88.

Thomas, R.J., Jacobs, J., Falter, M. and Jessberger, A. (1996): K-Ar and Ar-Ar dating of mineral separates from the Natal metamorphic province. Geol. Surv. S. Afr. Ann. Techn. Rep., **1995**, 52–56.

Williams, I.S. and Claesson, S. (1987): Isotopic evidence for the Precambrian provenance and Caledonian metamorphism of high grade paragneisses from the Seve Nappes, Scandinavian Caledonides II: Ion microprobe zircon U-Th-Pb. Contrib. Mineral. Petrol., **97**, 205–217.

Wuth, M.G. and Archer, P.D. (1986): Chromite mineralization at Sithilo, Northern Zululand. Mineral Deposits of Southern Africa, ed. by C. R., Anhaeusser and S., Maske. Johannesberg, Geological Society of South Africa, Vol.2, 1689–1694.